

Article

Effect of Friction Stir Processing on Microstructural, Mechanical, and Corrosion Properties of Al-Si12 Additive Manufactured Components

Ghazal Moeini ^{1,*}, Seyed Vahid Sajadifar ² , Tom Engler ³, Ben Heider ³ , Thomas Niendorf ² , Matthias Oechsner ³ and Stefan Böhm ¹

¹ Department for Cutting and Joining Processes, University of Kassel, Kurt-Wolters-Str. 3, 34125 Kassel, Germany; s.boehm@uni-kassel.de

² Institute of Materials Engineering, University of Kassel, Moenchebergstraße 3, 34125 Kassel, Germany; sajjadifar@uni-kassel.de (S.V.S.); niendorf@uni-kassel.de (T.N.)

³ Center for Structural Materials (MPA-IfW), Technical University of Darmstadt, Grafenstraße 2, 64283 Darmstadt, Germany; engler@mpa-ifw.tu-darmstadt.de (T.E.); heider@mpa-ifw.tu-darmstadt.de (B.H.); oechsner@mpa-ifw.tu-darmstadt.de (M.O.)

* Correspondence: g.moeini@uni-kassel.de; Tel.: +49-561-804-7443

Received: 12 December 2019; Accepted: 31 December 2019; Published: 3 January 2020



Abstract: Additive manufacturing (AM) is an advanced manufacturing process that provides the opportunity to build geometrically complex and highly individualized lightweight structures. Despite its many advantages, additively manufactured components suffer from poor surface quality. To locally improve the surface quality and homogenize the microstructure, friction stir processing (FSP) technique was applied on Al-Si12 components produced by selective laser melting (SLM) using two different working media. The effect of FSP on the microstructural evolution, mechanical properties, and corrosion resistance of SLM samples was investigated. Microstructural investigation showed a considerable grain refinement in the friction stirred area, which is due to the severe plastic deformation and dynamic recrystallization of the material in the stir zone. Micro-hardness measurements revealed that the micro-hardness values of samples treated using FSP are much lower compared to SLM components in the as-built condition. This reduction of hardness values in samples treated with FSP can be explained by the dissolution of the very fine Si-phase network, being characteristic for SLM samples, during FSP. Surface topography also demonstrated that the FSP results in the reduction of surface roughness and increases the homogeneity of the SLM microstructure. Decreased surface roughness and grain size refinement in combination with the dissolved Si-phase network of the FSP treated material result in considerable changes in corrosion behavior. This work addresses the corrosion properties of surface treated additive manufactured Al-Si12 by establishing adequate microstructure-property relationships. The corrosion behavior of SLM-manufactured Al-Si12 alloys is shown to be improved by FSP-modification of the surfaces.

Keywords: additive manufacturing; friction stir processing; microstructure; corrosion

1. Introduction

Technology to produce components with high efficiency and functional properties in a relatively short time and at lower costs is the main demand of most industries. Additive manufacturing (AM) as a direct manufacturing technology provides the opportunity to produce high-performance components characterized by complex geometry directly from computer-aided design (CAD) data. Selective laser melting (SLM) is the powder bed fusion additive manufacturing technique most frequently used for AM of aluminum alloys [1]. SLM can produce near-net-shaped objects with superior dimensional accuracy

and an overall higher quality compared to other AM techniques. However, due to the layer-wise nature of additive manufacturing, the components show poor surface quality. To improve the surface quality, different aspects related to AM processing as well as post-processing techniques were studied [2–12]. Calignano et al. [2] studied the effect of the direct metal laser sintering (DMLS) process parameters such as scan speed, laser power and hatching distance on the surface roughness of AlSi10Mg components. Results showed that laser scan speed plays an important role in the surface roughness of as-built parts. Townsend et al. [3] observed that the disappearance of laser tracks on the side surface of the AlSi10Mg SLM parts leads to lower values of surface roughness as compared to that of the top surface. Furthermore, diverse thermal post-processing and surface treatment techniques, e.g., shot peening, were used to enhance the surface quality. Shot peening leads to localized plastic deformation on the surface layer promoting the evolution of compressive residual stress. This eventually improves the mechanical properties and fatigue strength of AM components [5,8,9]. The effect of laser shot peening on the fatigue properties of AM 316L samples was investigated elsewhere [4]. It was reported that the deep level of plastic deformation introduced by the laser shot peening process can considerably enhance the fatigue strength. Maamoun et al. [5] demonstrated the improvement of surface integrity, microstructure homogeneity and mechanical properties of AlSi10Mg SLM surfaces after applying shot peening treatments. The effective depth of shot peening was reported to be in the range of 100 to 200 μm .

Establishing an adequate post-processing technique to simultaneously achieve high strength, high surface quality, minimal porosity and high corrosion resistance in AM parts has always been the aim of research. Zakay et al. [6] studied the impact of post-process heat treatments on the corrosion behavior of AlSi10Mg SLM samples. They studied the general corrosion behavior by salt spray testing and electrochemical impedance spectroscopy as well as the stress corrosion cracking behavior by low cycle corrosion fatigue. It was reported that the heat treated samples (200–300 $^{\circ}\text{C}$ for 2 h) showed a relatively enhanced corrosion resistance. This was attributed to the preservation of the fine Si cellular morphology embedded in the aluminum matrix that was achieved during SLM processing.

Friction stir processing (FSP) is a commonly applied post-treatment technique for microstructural modification and improvement of surface quality in a localized area [13,14]. In FSP, a rotating tool with pin and shoulder is inserted into the material and traversed along the desired path in order to extensively mix the material in the processing area. The influence of FSP on the microstructural modification and mechanical properties of as-cast Al-Si-Mg alloys was numerously studied, e.g., in [15,16]. The results revealed that FSP can be used to improve the mechanical properties of components by grain refinement and reduction of casting porosity. Another study [16] also showed that the FSP improves the intergranular corrosion resistance of Al5083 alloy by refining the microstructure and partial dissolution of precipitates in the FSP treated area. Macias et al. [17] investigated the noticeable effect of FSP on microstructural refinement, porosity reduction and fatigue enhancement of SLM AlSi10Mg. Maamoun et al. [10] applied FSP as a localized surface treatment for additively manufactured AlSi10Mg. Their investigations revealed that the FSP is able to break up the fibrous Si network being characteristic for the as-built SLM samples into nano-scale particles, resulting in a more homogeneous distribution of nano-scale Si particles. Additionally, FSP can efficiently reduce porosity in the stir zone and also can have a pronounced in-depth effect [10]. In light of the presented findings, FSP can be regarded as an effective post-treatment technique to improve the surface quality and promote microstructure refinement. However, there are still only a few studies dealing with the effect of FSP on the mechanical and corrosion behavior of aluminum alloys and Al-12Si, respectively, fabricated via SLM. Therefore, the main objective of this study is to establish a bridge between FSP, microstructural variations and corrosion behavior of Al-Si12 fabricated via the SLM process.

2. Materials and Methods

Samples of Al-Si12 alloy were manufactured using a commercially available SLM system SLM 280^{HL}, distributed by SLM Solutions, Lübeck, Germany. The machine is equipped with a 400 W

ytterbium fiber laser with a spot size of 85 μm . The commercially available powder material Al-Si12 (Wt.%) was used to manufacture samples in an inert environment using argon gas. The parameters used for manufacturing the sample volume were: scanning speed 1200 mm/s, laser power 350 W, layer thickness 50 μm and hatch spacing 190 μm . The SLM samples with a size of 60 mm \times 25 mm \times 5 mm were friction stir processed. An FSP tool with a 10 mm shoulder and no pin was used in this study. FSP was conducted employing parameters as follows: rotational speed 1800 rotations per minute, travel speed 160 mm/min and 0.1 mm tool penetration. The Friction stir process was carried out with appropriate clamping and fixing settings. FSP was conducted in two types of working media, in air and under water. In the latter case, the samples were fixed in a water container. The water level was about 25 mm above the sample surface. Processing direction was parallel to the SLM build direction (BD). To distinguish between samples, the samples were labeled as follows: AC for FSP in air and UW for FSP in water. Standard mechanical grinding and polishing procedures were used to prepare samples for microstructural analysis. Optical microscopy (OM) and a scanning electron microscope (SEM)/(Carl Zeiss AG, Jena, Germany), equipped with an electron backscatter diffraction (EBSD) unit were employed to characterize the microstructure of the samples. For EBSD measurements, samples were prepared by 24 h of vibro-polishing in a colloidal silica solution (OPS). Vickers micro-hardness testing was performed using a KB 30S Vickers hardness tester (KB Prüftechnik, Hochdorf-Assenheim, Germany) with a diamond indenter in the shape of a pyramid. A force of 0.3 N was applied for 10 s on the surface of the samples according to the standard, ASTM: E384-11e1. Optical topography measurements of the SLM surfaces before and after the FSP were performed using MicroProf[®] (FRT GmbH, Bergisch Gladbach, Germany). To investigate the influence of FSP on corrosion properties, the samples were tested according to DIN EN ISO 11846:2008-08, which is the standard to be used for determination of the resistance against intergranular corrosion of solution heat-treatable aluminum alloys. After initial preparation through etching in 5% sodium hydroxide (NaOH) at 50 °C for 2.5 min and subsequent neutralizing in 70% nitric acid (HNO₃) at ambient temperature for 2 min, the samples were immersed in a solution of 3% sodium chloride (NaCl) and 1% hydrochloric acid (HCl) for 24 h at ambient temperature. The volume to surface ratio was 5 ml/cm². After the test, corrosion products were removed by etching using nitric acid. Macroscopic documentation was performed using a Keyence VHX-6000 digital microscope (Keyence Corporation, Osaka, Japan). Metallographic investigations were performed on the Cross-sections of the studied samples.

3. Results and Discussion

3.1. Microstructural Evolution

From the SEM micrographs of the samples, focusing on the SLM as-built condition as well as the stir zone and the thermomechanically affected zone (TMAZ) upon FSP (Figure 1), it can be deduced that a Si-rich network of cellular shape is present in the SLM aluminum matrix. However, upon FSP, the Si network is completely dissolved and transformed into Si-rich particles. The microstructure of the AC-FSP state is characterized by spheroidized Si-rich particles, with relatively high inter-particle distance, while in the UW-FSP state the Si-rich particles are significantly finer and different in shape, i.e., mostly acicular. Dissolution of the Si-rich network was also seen after friction stir welding (FSW) of SLM Al-Si12 elsewhere [18]. Severe plastic deformation, fragmentation, and dynamic recrystallization during FSP and FSW, respectively, are known to be able to dissolve the network formed previously in the SLM process.

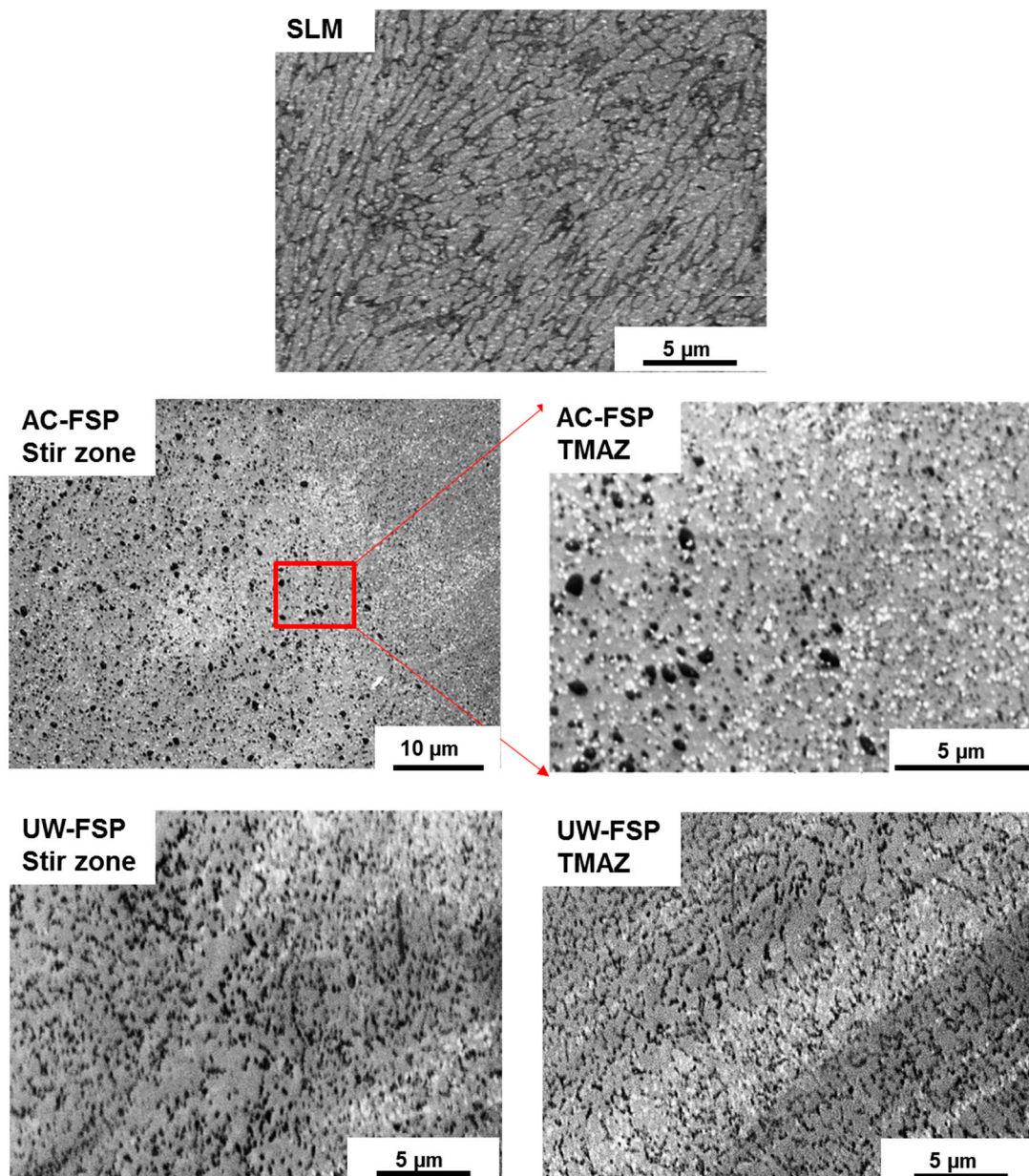


Figure 1. Micrographs (SE contrast) of SLM, AC-FSP and UW-FSP samples.

The microstructure of Al-Si12 samples in different conditions was further characterized via EBSD. EBSD micrographs (inverse pole figure (IPF) maps) of the alloy before and after FSP processing are shown in Figure 2. The step sizes of EBSD measurements for SLM, AC-FSP and UW-FSP samples were 200 nm, 500 nm and 20 nm, respectively. Evidently, the FSP processing of SLM processed Al-Si12 leads to grain refinement. Grain refinement is due to both severe plastic deformation and dynamic recrystallization of the material during FSP [13]. It is also worth noting that the level of grain refinement is more pronounced for the sample processed underwater (UW-FSP) compared to the sample processed in air (AC-FSP). Since heat transfer is enhanced in the water environment, there is less time for the growth of newly recrystallized grains in UW-FSP. Therefore, lower grain size and a higher level of grain refinement, respectively, are seen upon underwater FSP treatment.

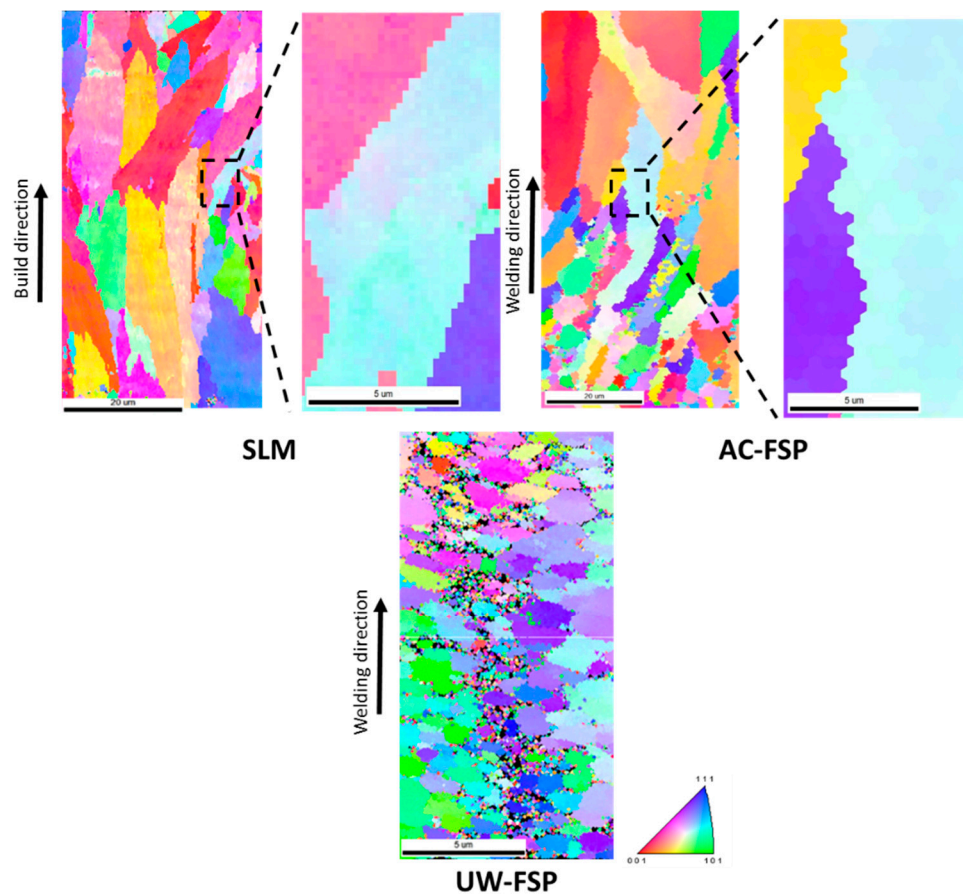


Figure 2. EBSD micrographs of SLM, AC-FSP and UW-FSP samples; color coding is in line with the standard triangle shown to the lower right.

3.2. Hardness and Topography

Vickers micro-hardness was measured on the surface of the differently treated samples, Table 1 and Figure 3. A decrease in the Vickers micro-hardness values of AC samples was found. This can be rationalized based on the microstructural evolution, i.e., the dissolution of the initial Si network followed by coarsening of the Si precipitates. Most importantly, due to the high cooling rate in the case of UW-FSP samples, the micro-hardness remains on a medium level as compared to the other two conditions. By using water as the convective medium, frictional heat can effectively be dissipated. This hampers microstructural changes and coarsening of microstructural features in the FSP treated area to a certain degree. Eventually, underwater FSP can improve the mechanical properties.

Table 1. Vickers micro-hardness values of SLM, AC-FSP and UW-FSP samples (HV 0.3).

SLM	AC-FSP	UW-FSP
115-123 HV	78-95 HV	97-112 HV

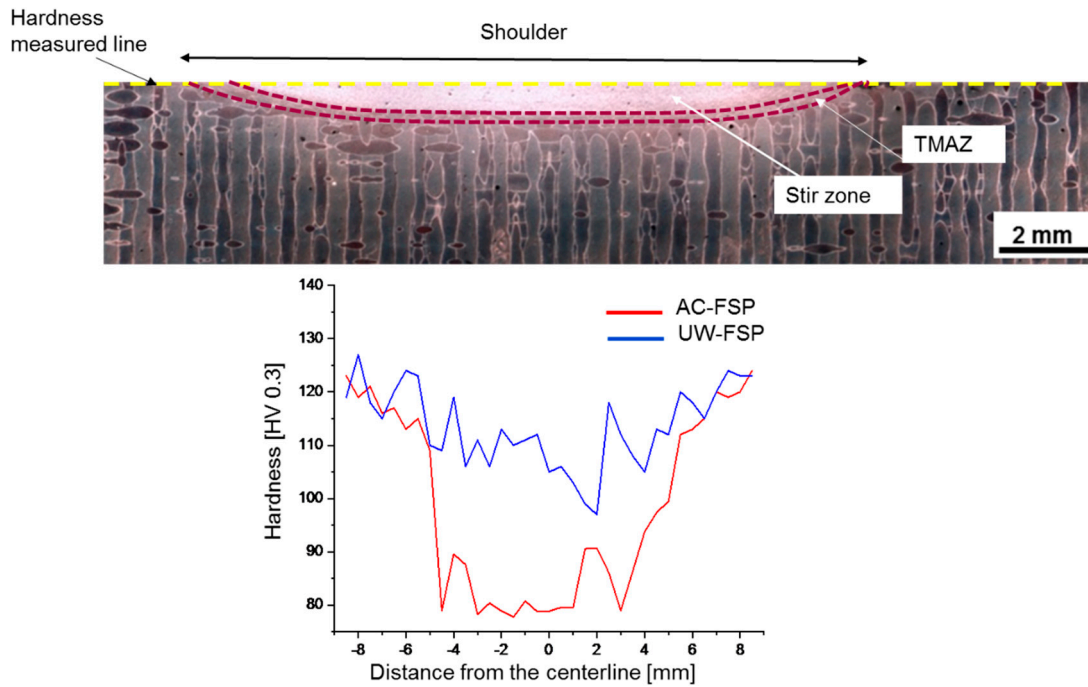


Figure 3. Hardness distribution along the FSP treated surfaces in AC-FSP and UW-FSP conditions.

The surface roughness measurements of samples in different conditions (as-built, AC-FSP and UW-FSP) are shown in Figure 4. It can be seen that relatively poor surface quality is found in the case of the as-built SLM sample. On FSP surfaces the surface roughness was significantly reduced and the pattern became quite uniform.

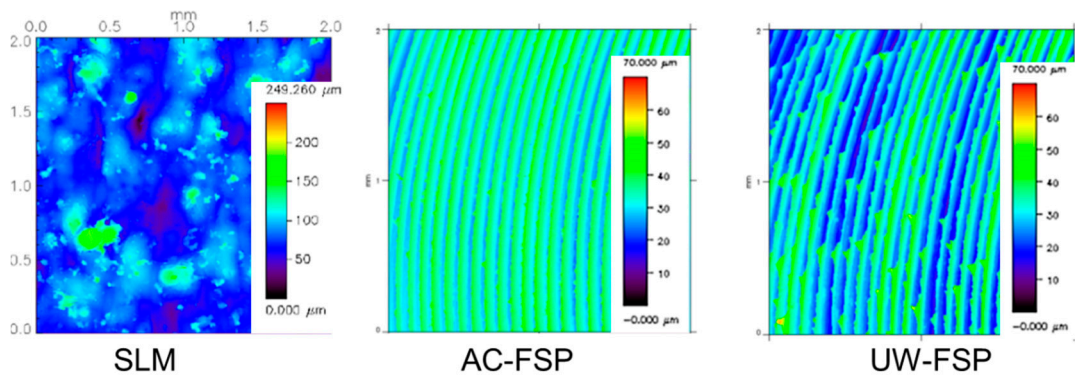


Figure 4. Surface topography obtained by optical measurements on the surface of samples in different conditions.

3.3. Corrosion Behavior

Without FSP-modification of the surface, the as-built SLM-manufactured sample appears intact; however, traces of a corrosive attack are observed between the individual laser scanning paths, cf. Figure 5. It seems that the interfaces between individual layers are preferential corrosion sites. This can be rationalized based on local changes in microstructural appearance and distribution of elements, as can be deduced from the locally different shapes of the Si-rich networks, in each single layer and scan track (Figure 6). The penetration depth of corrosion was found to be about 980 μm.

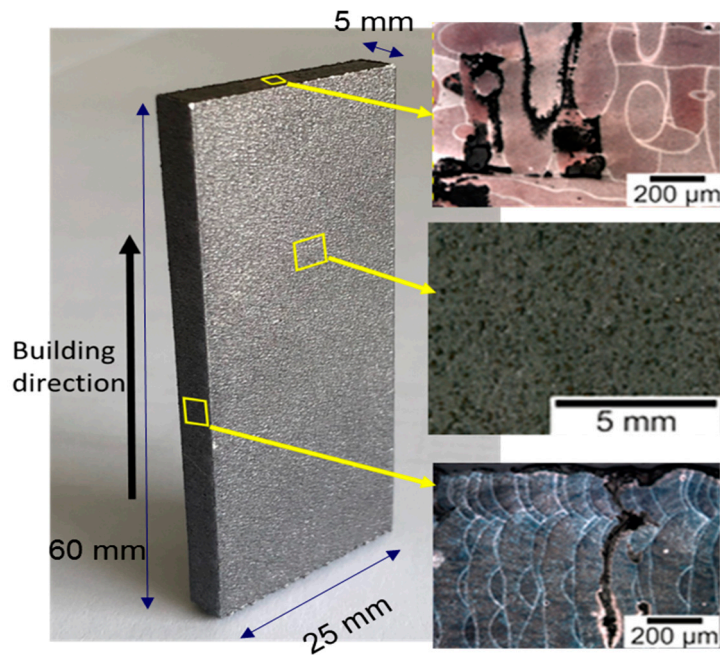


Figure 5. As-built SLM sample after corrosion testing. Left: Macroscopic documentation; Right: Cross-section perpendicular to build direction (top), corrosion attack at the large surface (middle), corrosion attack in the smaller surface (bottom).

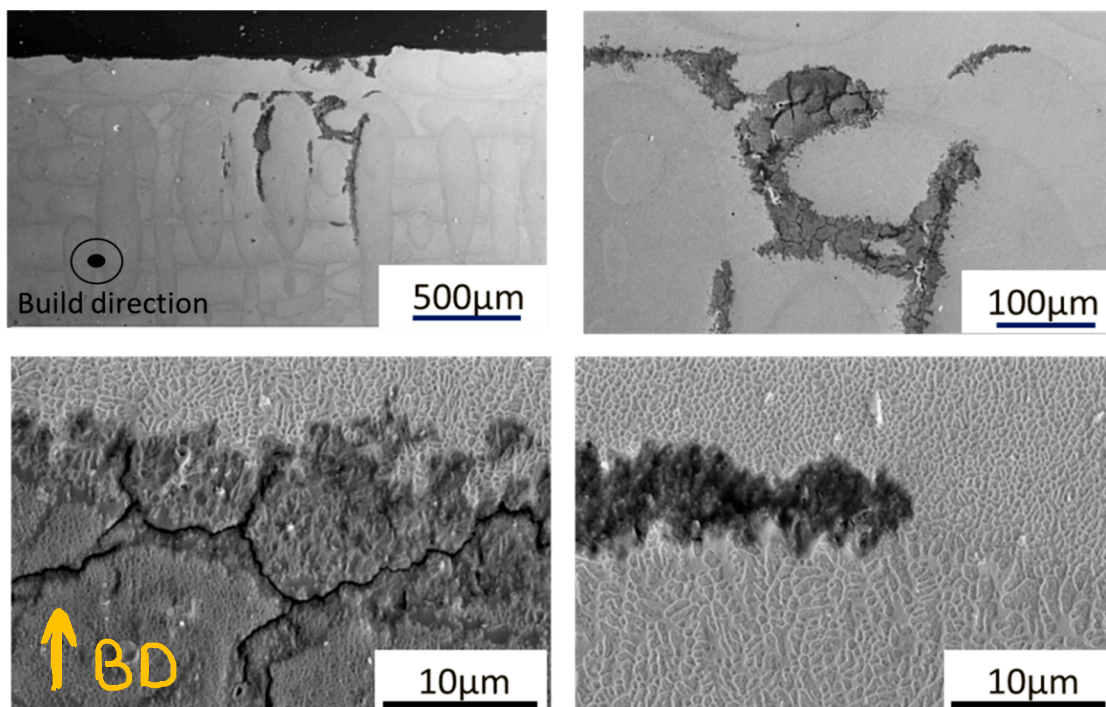


Figure 6. SEM micrographs of the cross-section of the as-built SLM sample after corrosion testing.

The FSP zones of the samples processed under water (UW-FSP) and in air (AC-FSP) corroded as well during 24 h of immersion in 3% NaCl with 1% HCl. However, there are obvious differences in the corrosion resistance of the different zones in the FSP samples, as well as alongside the direction of tool movement during FSP treatment. Both samples corroded severely at the boundary between the FSP zone and the SLM base metal, while most of the FSP zone is still intact and, in most of the area, without any traces of corrosion damage. The FSP-modified zone of the AC-FSP sample, as shown in Figure 7, is intact up to about 10 mm from the starting position of the FSP treatment. After that, corrosion marks

appear in the middle of the modified surface area and the corrosive attack between the FSP zone and SLM base metal on the advancing side intensifies. Pitting corrosion occurred within the FSP zone, while it seems that selective corrosion of the boundary between the FSP zone and the SLM base metal prevails. The latter could have been initiated as galvanic corrosion due to the difference in microstructures and elemental distribution, respectively, of the two adjacent zones. Progressive degradation seems to be further driven by pitting and/or crevice corrosion. With the FSP zone remaining intact, the prevalent corrosion type leads to the undercutting of that zone. Maximum corrosion depth within the FSP zone is 312 μm .

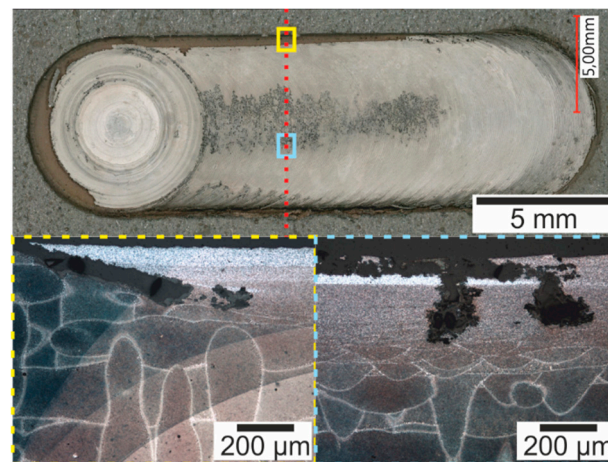


Figure 7. AC-FSP sample after corrosion testing. Top: Macroscopic documentation; Bottom: Cross-sections: perpendicular to processing direction within the boundary region (left) and middle of the FSP zone (right).

Large areas of the UW-FSP-modified zone were dissolved during the corrosion test (Figure 8). These zones are located at the starting point of the FSP zone and within the outer areas, where the retreating side seems to be more deteriorated. The middle of the FSP zone seems to be fully intact after the corrosion test. The same holds true for the end of the FSP zone. At these spots there are no signs of localized corrosion. Within the transition area between the FSP zone and the SLM base metal, a similar corrosion appearance is observed in the cross-section as in case of the AC-FSW sample; however, the edge of the FSP zone seems to be more severely deteriorated upon UW-FSP. The maximum observed corrosion depth in the transition area is 260 μm .

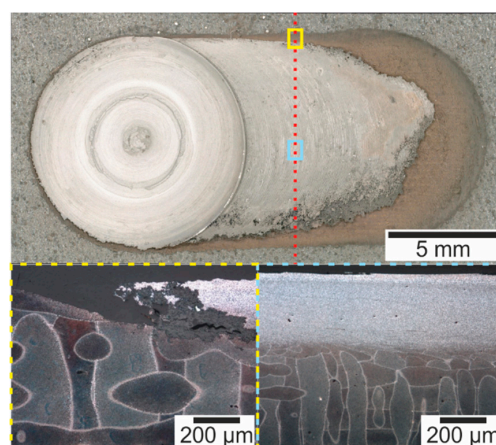


Figure 8. UW-FSP sample after corrosion testing. Top: Macroscopic documentation; Bottom: Cross-sections perpendicular to processing direction within the boundary region (left) and middle of the FSP zone (right).

In the SEM micrographs recorded in the transition area between the FSP zone and the as-built SLM microstructure, significant corrosion activity is seen (Figure 9). The FSP surface is characterized by a wavy surface appearance, while the SLM surface is significantly rougher. Previous melt pools in the as-built SLM material can be perceived clearly in the high-resolution image. In between both areas there is a zone, where the shape of the melt pools is distorted. This zone is affected by the severe deformation induced by the movement of the FSP tool on the surface. While the surface of the FSP zone is almost free of corrosion induced changes, the transition zone is severely deteriorated upon the corrosion test. The reason for this is seen in the microstructural and compositional differences between the two adjacent zones: While the Si-rich network of cellular shape is intact in the unaffected melt pools, i.e., sample regions without any FSP induced distortion, the Si-rich network is transformed into Si-rich particles embedded in an aluminum matrix in the FSP zone. Both microstructures show good corrosion resistance; however, the transition area, i.e., the TMAZ, where an intermediate state featuring ill-defined network structures and partially grown Si-rich precipitates prevails (cf. Figure 1), is obviously highly susceptible to corrosion.

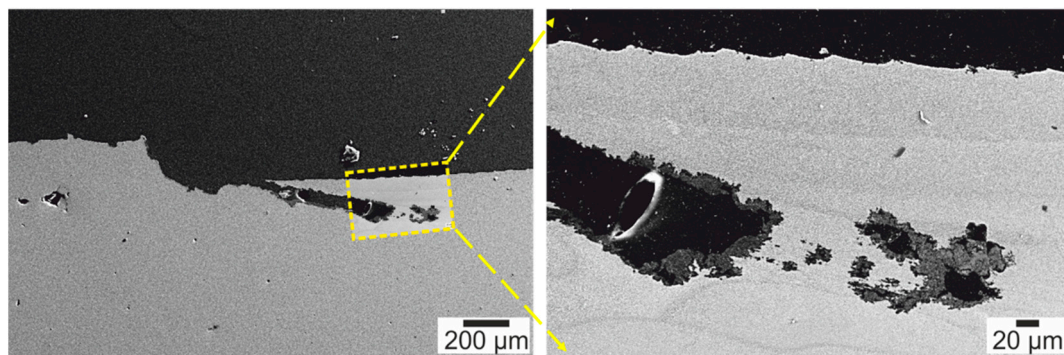


Figure 9. SEM-image of the transition area between the FSP zone and as-built SLM microstructure of the AC-FSP sample: the high-resolution micrograph (right hand side) is taken from the area marked by the yellow square.

The maximum corrosion depth was significantly reduced through FSP-modification of the SLM-manufactured samples. However, corrosion still occurred on the surface of the FSP-modified samples. By direct comparison of the final appearance of the differently treated samples, it seems to be possible to deduce the mechanisms leading to the differing kinds of corrosive attack. Assuming that lower cooling rates and, eventually, higher heat input are effective during AC-FSP, it is expected that larger TMAZ and heat affected zones (HAZ) prevail, finally increasing the undercutting depth below the rather undamaged FSP zone. Furthermore, the continued heat input during FSP seems to lead to sensitization of the already modified surface. In UW-FSP the higher cooling rates and absorbed excess heat seem to improve the corrosion resistance of the FSP zone. The reason for this may be, among others, the smaller size and larger distance between the Si-rich precipitates. However, due to the smaller TMAZ and HAZ, the gradient in electrochemical potential is higher, eventually leading to increased dissolution of the boundary region, severe undercutting and strongly promoted dissolution of the FSP-modified surface. This is, presumably, the reason for the areal dissolution in vicinity of the starting point of the FSP zone. For in-depth analysis of the underlying mechanisms and their interplay; however, further work is needed, focusing for example on microstructural homogeneity in the FSP affected zones as well on direct determination of local electrochemical potentials. Results will be published in follow-up studies.

4. Conclusions

Friction stir processing (FSP) technique was employed to enhance the surface quality and homogenize the microstructure of Al-Si12 samples produced by selective laser melting (SLM). FSP was carried out in two different environments i.e., water and air, to investigate the effect of cooling rate

during processing. Microstructural evolution, as well as surface roughness and corrosion behavior of both FSP treated and SLM as-built samples were explored. The following conclusions can be drawn from the results presented:

1. SEM analysis revealed that the microstructure of SLM processed samples is characterized by Si-rich networks in the Al matrix. These networks were dissolved upon FSP treatment and replaced with spheroidized Si-rich particles. The size of these particles is larger for the sample FSP treated in air as compared to the condition processed in water.
2. EBSD measurements confirmed that grain refinement took place during FSP of additively manufactured Al-Si12. The degree of refinement was seen to be higher for the sample processed in water.
3. The corrosion behavior of SLM-manufactured AlSi12 alloys can be improved by the FSP-modification of the surfaces. The corrosion performance within the FSP treated zone is thought to be affected by several mechanisms, among others by the anodic dissolution of the Al matrix due to the occurrence of Si-rich precipitates in these zones.
4. Higher cooling rates being characteristic for UW-FSP seem to lead to a microstructure with higher corrosion resistance as compared to AC-FSP.

More detailed investigations with a more localized exposition to corrosive media are required to fully understand the interaction between the different zones induced by FSP in corrosive environments.

Author Contributions: Conceptualization, G.M.; Methodology, S.V.S., G.M., B.H. and T.E.; Validation, G.M.; Investigation, S.V.S., B.H., T.E., G.M.; Writing-Original Draft Preparation, G.M.; Writing-Review & Editing, G.M., T.N.; Visualization, G.M.; Supervision, S.B., T.N. and M.O. All authors have read and agreed to the published version of the manuscript.

Funding: The authors are grateful for the support from the Hessen State Ministry for Higher Education, Research and the Arts-Initiative for the Development of Scientific and Economic Excellence (LOEWE) for the ALLEGRO project.

Conflicts of Interest: The authors declare no conflict of interest.

References

1. Frazier, W.E. Metal additive manufacturing: A review. *J. Mater. Eng. Perform.* **2014**, *23*, 1917–1928. [[CrossRef](#)]
2. Calignano, F.; Manfredi, D.; Ambrosio, E.P.; Iuliano, L.; Fino, P. Influence of process parameters on surface roughness of aluminum parts produced by DMLS. *Int. J. Adv. Manuf. Technol.* **2013**, *67*, 2743–2751. [[CrossRef](#)]
3. Townsend, A.; Senin, N.; Blunt, L.; Leach, R.K.; Taylor, J.S. Surface texture metrology for metal additive manufacturing: A review. *Precis. Eng.* **2016**, *46*, 34–47. [[CrossRef](#)]
4. Hackel, L.; Rankin, J.R.; Rubenchik, A.; King, W.E.; Matthews, M. Laser peening: A tool for additive manufacturing post-processing. *Addit. Manuf.* **2018**, *24*, 67–75. [[CrossRef](#)]
5. Maamoun, A.; Elbestawi, M.; Veldhuis, S. Influence of Shot Peening on AlSi10Mg Parts Fabricated by Additive Manufacturing. *J. Manuf. Mater. Process.* **2018**, *2*, 40. [[CrossRef](#)]
6. Zakay, A.; Aghion, E. Effect of Post-Heat Treatment on the Corrosion Behavior of AlSi10Mg Alloy Produced by Additive Manufacturing. *JOM* **2019**, *71*, 1150–1157. [[CrossRef](#)]
7. Lamikiz, A.; Sánchez, J.A.; López de Lacalle, L.N.; Arana, J.L. Laser polishing of parts built up by selective laser sintering. *Int. J. Mach. Tools Manuf.* **2007**, *47*, 2040–2050. [[CrossRef](#)]
8. AlMangour, B.; Yang, J.-M. Improving the surface quality and mechanical properties by shot-peening of 17-4 stainless steel fabricated by additive manufacturing. *Mater. Des.* **2016**, *110*, 914–924. [[CrossRef](#)]
9. Uzan, N.E.; Ramati, S.; Shneck, R.; Frage, N.; Yeheskel, O. On the effect of shot-peening on fatigue resistance of AlSi10Mg specimens fabricated by additive manufacturing using selective laser melting (AM-SLM). *Addit. Manuf.* **2018**, *21*, 458–464. [[CrossRef](#)]
10. Maamoun, A.H.; Veldhuis, S.C.; Elbestawi, M. Friction stir processing of AlSi10Mg parts produced by selective laser melting. *J. Mater. Process. Tech.* **2019**, *263*, 308–320. [[CrossRef](#)]

11. Kumbhar, N.N.; Mulay, A.V. Post Processing Methods used to Improve Surface Finish of Products which are Manufactured by Additive Manufacturing Technologies: A Review. *J. Inst. Eng. Ser. C* **2018**, *99*, 481–487. [[CrossRef](#)]
12. Ahmed, H.; Stephen, C. Post-processing of the additively manufactured AlSi10Mg parts produced by Selective Laser Melting. In Proceedings of the The 7th International Conference on Virtual Machining Process Technology, Hamilton, ON, Canada, 7–9 May 2018; pp. 5–6.
13. Lathabai, S.; Migeon, R.; Tyagi, V.K.; O'Donnell, R.G.; Estrin, Y. Friction Stir Processing: A Technique for Microstructural Refinement in Metallic Materials. *Mater. Sci. Forum* **2009**, *618–619*, 63–67. [[CrossRef](#)]
14. Mishra, R.S.; Ma, Z.Y. Friction stir welding and processing. *Mater. Sci. Eng. R Rep.* **2005**, *50*, 1–78. [[CrossRef](#)]
15. Ma, Z.Y.; Sharma, S.R.; Mishra, R.S. Microstructural modification of As-cast Al-Si-Mg alloy by friction stir processing. *Metall. Mater. Trans. A Phys. Metall. Mater. Sci.* **2006**, *37*, 3323–3336. [[CrossRef](#)]
16. Abdi behnagh, R.; Besharati Givi, M.K.; Akbari, M. Mechanical properties, corrosion resistance, and microstructural changes during friction stir processing of 5083 aluminum rolled plates. *Mater. Manuf. Process.* **2012**, *27*, 636–640. [[CrossRef](#)]
17. Santos Macias, J.G.; Van Hooreweder, B.; Maire, E.; Adrien, J.; Jacques, P. Friction stir processing of additive manufactured AlSi10Mg parts to improve mechanical behaviour. In Proceedings of the FSWP 2017—5th International Conference on Scientific and Technical Advances on Friction Stir Welding & Processing, Metz, France, 11–13 October 2017.
18. Moeini, G.; Sajadifar, S.V.; Wegener, T.; Brenne, F.; Niendorf, T.; Böhm, S. On the low-cycle fatigue behavior of friction stir welded Al-Si12 parts produced by selective laser melting. *Mater. Sci. Eng. A* **2019**, *764*, 138–189. [[CrossRef](#)]



© 2020 by the authors. Licensee MDPI, Basel, Switzerland. This article is an open access article distributed under the terms and conditions of the Creative Commons Attribution (CC BY) license (<http://creativecommons.org/licenses/by/4.0/>).